LA-UR -85-2670

CONF-8508100--1

Los Alamos National Laboratory is operated by the University of California for the United States Department of Energy under contract W-7405-ENG-36

LA-UR--85-2670

DE85 015740

TITLE: Configuration Space Methods in the Three-Nucleon Problem

AUTHOR(S): James L. Friar

SUBMITTED TO: Invited lecture presented at the "International Symposium on Few-Body Methods," Nanning, People's Republic of China, August 4-10, 1985.

DISCLAIMER

Los Alamos Los Alamos National Laboratory
Los Alamos, New Mexico 87545

FORM NO 836 R4

CONFIGURATION SPACE METHODS IN THE THREE-NUCLEON PROBLEM

J. L. Friar

Theoretical Division
Los Alamos National Laboratory
Los Alamos, NM 87545 USA

ABSTRACT

The assumptions underlying the formulation and solution of the Schrödinger equation for three nucleons in configuration space are reviewed. Those qualitative aspects of the two-nucleon problem which play an important role in the trinucleon are discussed. The geometrical aspects of the problem are developed, and the importance of the angular momentum barrier is demonstrated. The Faddeev-Noyes formulation of the Schrödinger equation is motivated, and the boundary conditions for various three-body problems is reviewed. The method of splines is shown to provide a particularly useful numerical modelling technique for solving the Faddeev-Noyes equation. The properties of explicit trinucleon solutions for various two-body force models are discussed, and the evidence for three-body forces is reviewed. The status of calculations of trinucleon observables is discussed, and conclusions are presented.

1. INTRODUCTION

The four bound few-nucleon systems (^{2}H, ^{3}H, ^{3}He, ^{4}He) have played a role in nuclear physics far out of proportion to their abundance on the earth, and their study constitutes one of the oldest and most important subfields of that discipline. In one of the first review articles treating nuclear physics[1]), a separate section was reserved

for the few-nucleon problem. Since that time many such articles have been written, and many symposia like the current one have been held.

The special importance of these four nuclei stems from the great difficulty in solving the many-body problem. Special techniques exist for solving that problem when the number of particles becomes huge, a limit of no particular relevance to nuclear physics. On the other hand we can also solve "exactly" (in the numerical sense) well-posed model problems with four or fewer nucleons. Our lack of ability to construct from first principles a tractable Hamiltonian for the interaction of a single pair of nucleons which describes all the phenomena associated with this system means that we routinely use semiphenomenological Hamiltonians, which incorporate physical constraints and some parameters which are fitted to two-nucleon experimental data. Thus, the three- and four-nucleon systems constitute a special testing ground for new ideas and concepts in nuclear physics, simply because we can solve for their wave functions and because their properties have not been incorporated into our Hamiltonian models.

Although much of the modern work in our field is formulated in momentum space, most of the older work and the work described in this lecture were formulated in configuration space (CS). Many techniques have been used to calculate CS wave functions, beginning with the august Rayleigh-Ritz variational principle[1]). Most methods expand the wavefunction into well-defined components and solve for the amounts of these components. The modern variational calculations[2]), the hyperspherical harmonic method[3]), and our own work fall[4]) into this category. The powerful Green's function Monte Carlo method[5]) is the one exception.

Why do we and others work in configuration space? In our case the answer is simple: our physical intuition and insight are greatest there. There are, however, distinct advantages to momentum space for certain problems, such as relativistic treatments of few-nucleon systems. In what follows we will emphasize almost exclusively the bound few-nucleon systems in configuration space, and the approach of the Los Alamos-Iowa collaboration to solving the Schrödinger equation for these systems.

2. TWO-NUCLEON PROBLEM

No discussion of the three-nucleon problem is complete without a schematic discussion of the two-nucleon Hamiltonian. Many of the detailed quantitative features are irrelevant, while a few seemingly unimportant qualitative features determine most of the trinucleon properties.

The key underlying assumption is that few-nucleon dynamics is nonrelativistic. This important simplification relies on the fact that typical values of mean internal nuclear momenta, $\bar{p}$, are 100-200 MeV/c, and thus $(v/c)^2 = (\bar{p}/Mc)^2$ for a nucleon of mass M=939 MeV is one-few percent. Since $(v/c)^2$ gives the scale of relativistic corrections, this estimate would indicate that a nucleus is largely nonrelativistic. The argument hides the fact that short-range potentials can be very strong and induce local momenta which are correspondingly large; the estimate above should only be interpreted as "in the mean". Moreover, our potential models "hide" the effects of relativity in the phenomenological parts.

There are three salient features of the two-nucleon potential which drastically, and unfavorably, affect our ability to solve the few-nucleon Schrödinger equation. These are:

(1) forces between like nucleons (e.g., pp or nn) are weaker than the forces between unlike nucleons (np);
(2) the two-nucleon spin-triplet potential contains a strong tensor force which couples neighboring orbital waves;
(3) the short-range force exhibits very strong repulsion, which makes the probability of nucleon-nucleon overlap at short distances very small.

Without these complications, the few-nucleon Schrödinger equation is nearly as easy to solve as the corresponding atomic physics problem (He atom). Feature (1) induces important spin and isospin correlations in the wave function. If the forces between all particles were identical, only a single (different) scalar function of the particle separations would describe each of the few-nucleon systems. With a tensor force present, the deuteron wave function has a tensor (d-wave) component, as do the triton and α-particle, which greatly complicates solving the

Schrödinger equation. A strong short-range repulsion produces "holes" in the wave function. These holes must be accurately generated in any solution, which is thus rendered considerably more difficult.

In addition to these qualitative aspects of the nucleon-nucleon force, we note also that the odd-parity nucleon-nucleon partial waves (e.g., $^1P_0$, $^3P_{0,1,2}$) are relatively weak, and we will see later that they play a very small role in the triton.

3. BASIC PRINCIPLES AND THE GEOMETRY OF THE TRITON GROUND STATE

A few basic principles motivate the procedures used to solve numerically various three-body problems. These are:

(1) Nuclei (including the triton) are weakly bound, and average momenta are consequently small compared to the nucleon mass;
(2) In the triton the average momentum is comparable to the inverse of the radius (R) and consequently the angular momentum barrier suppresses higher partial waves of the nucleon-nucleon force;
(3) Unlike the case of heavy nuclei, the Pauli principle doesn't play a particularly large role;
(4) The details of the force are relatively unimportant in the overall binding, although they can severely complicate achieving a solution.

As we previously discussed, a nonrelativistic treatment of the triton should suffice, as indicated by (1). One estimate of the average momentum is $\bar{p} = \sqrt{ME_b} \equiv \hbar c\kappa$, where $E_b = 8.5$ MeV is the binding energy, and consequently, $\bar{p} \cong 90$ MeV/c. A typical trinucleon size is 2 fm, so that $\bar{p}R \sim 1$. Because Bessel functions of argument z and order ℓ peak for $z > \ell$, it is clear that the angular momentum barrier will greatly suppress orbital angular momenta greater than 2 in the triton.

The geometry of the triton illustrates the greater difficulty in solving the Schrödinger equation for the triton compared to the deuteron. The deuteron is described by a single vector $\vec{r}$ separating the nucleons, and only its magnitude is relevant for a description of the two scalar functions, u(r) and w(r), which determine the s-wave and d-wave parts of the wave function. Figure 1 shows the triton, where we have arbitrarily numbered the nucleons. Three points define a plane and thus only two vectors, $\vec{x}_1$ and $\vec{y}_1$, describe the system. Because

the orientation of the plane is arbitrary, only three independent interparticle coordinates (x_1, y_1, θ_1) are required to specify the wave function. Our choice of vectors is arbitrary, however, since any set of the Jacobi coordinates formed from the nucleon coordinates $\vec{r}_i$ (i, j, k cyclic) is adequate:

$$\vec{x}_i = \vec{r}_j - \vec{r}_k \quad , \tag{1}$$

$$\vec{y}_i = \frac{1}{2}(\vec{r}_j + \vec{r}_k) - \vec{r}_i \quad . \tag{2}$$

Clearly the sums of the $\vec{x}_i$ or $\vec{y}_i$ vanish and they are linearly dependent. Traditionally, the set $(\vec{x}_1, \vec{y}_1)$ is relabelled as $(\vec{x}, \vec{y})$, where $\vec{x}$ and $\vec{y}$ are denoted the "interacting pair" and "spectator" coordinates, respectively.

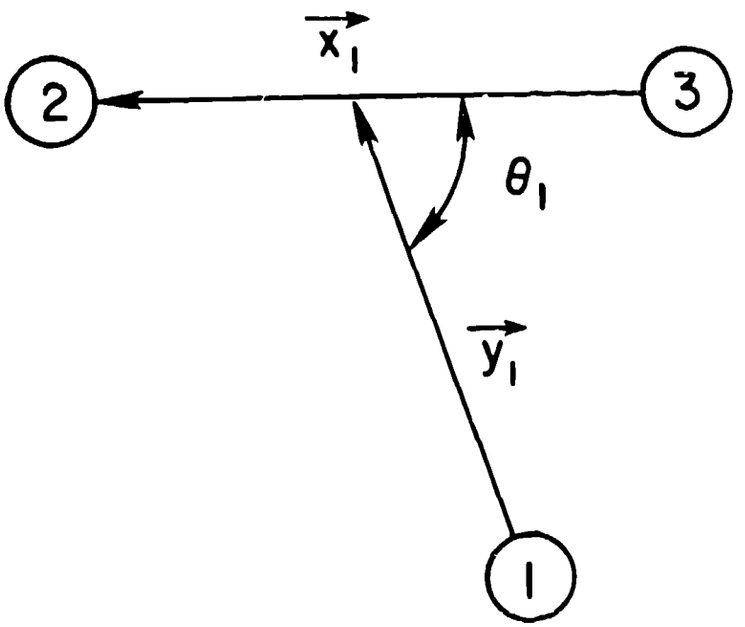

Figure 1. Jacobi coordinates (x_1, y_1, θ_1) for trinucleon problem.

Group theoretical methods are used to classify in a well-defined way[6]) the wave function components which can occur for the positive parity, spin-½ trinucleons. Most of the important qualitative aspects of this scheme are rather obvious, however. Like the deuteron, the principal triton wave function component is s-wave in character.

However, because there are several coordinates describing the problem, this can be further broken down into three distinct categories. (1) the S-state, completely symmetric under the interchange of spatial coordinates; (2) the S′-state, which has mixed spatial symmetry (neither symmetric nor antisymmetric); (3) the S′′-state which has spatial antisymmetry. The latter state has negligible size because the antisymmetry requires very large momentum components, which are lacking in the ground state, and because they are generated by the weak odd-parity nuclear forces. The S′-state vanishes when the np, nn, and pp forces are identical, and for this reason can be viewed as a space-isospin-(spin) correlation in the ground state. Its physical importance will be discussed later. The S-wave components are clearly spin doublet, since the trinucleons have spin ½; they are also iso-doublets if we ignore the Coulomb force in ^{3}He. There are also three independent spin-quartet D-state components, analogous to the deuteron case. Unlike the deuteron case, it is possible to construct a positive parity vector ($\hat{x} \times \hat{y}$), and this leads to three quartet and one doublet P-state components, which are very small. Adding everything together, there are 10 S-, P-, and D-state components, specified by 16 scalar functions.

The Schrödinger equation for the deuteron involves 2 coupled equations in one variable (r). The Schrödinger equation for the triton is a set of 16 coupled partial differential equations in 3 independent variables. This large number of equations makes the problem roughly equivalent to a single 4-variable problem, which would require heroic efforts, even for modern supercomputers. The way to circumvent this seemingly intractable situation is to use our knowledge of the physics of the problem: the angular momentum barrier suppresses many of the problem's complexities.

Figure 2 shows two of the energy scales of the triton. The upper graph illustrates the spin-and isospin-independent MT-V nucleon-nucleon potential model[7]), plotted versus nucleon-nucleon separation, x, and for comparison, the angular momentum part of the kinetic energy (for λ=2): $\hbar^2\ell(\ell+1)/Mx^2$. We see that the latter dwarfs the potential energy. Clearly, for higher values of ℓ this mismatch is even greater.

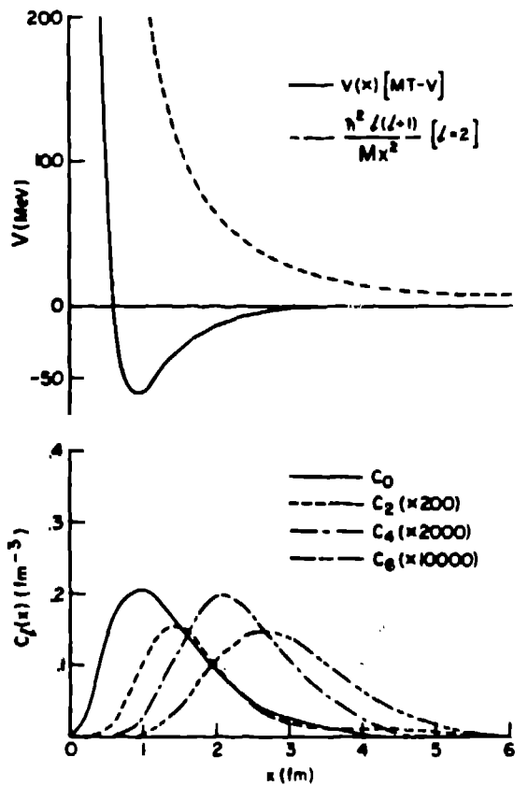

Figure 2. Comparison of centrifugal kinetic energy with the MT-V potential (top) and partial-wave projected triton correlation functions for that potential (bottom).

The implications for the binding of the triton are immediate: potential energy contributions for the higher nucleon-nucleon partial waves rapidly decrease as ℓ increases. We can easily see this by assuming a spin- and isospin-independent potential $V_{23}(x)$ between nucleons 2 and 3 and expanding this in a partial-wave series in both $\hat{x}$ and $\hat{y}$:

$$V_{23}(x) = \sum_{\alpha} |\alpha\rangle V_{23}(x) \langle\alpha| \quad , \tag{3}$$

where

$$|\alpha\rangle = [Y_{\ell}(\hat{x}) \mathbb{H} Y_{\ell}(\hat{y})]_0 \quad , \tag{4}$$

and the "channel"-label α is simply ℓ in this case. This series is much simpler than the general case, because we have assumed the same potential in every partial wave. Taking the expectation value of the potential between all three pairs of nucleons gives

$$\langle V \rangle = 3\langle V_{23}(x) \rangle \equiv 3\sum_{\ell} \int_0^{\infty} dx\, x^2 C_{\ell}(x) V_{23}(x) = \sum_{\ell} \langle V \rangle_{\ell} \quad , \tag{5}$$

where the partial-wave projected correlation function is

$$C_{\ell}(x) = \langle \alpha | \Psi \rangle (2\ell+1) \quad . \tag{6}$$

Only the completely space-symmetric S-state occurs in the wave function for this problem, and only even values of ℓ are nonvanishing because of this. The lower plot in fig. 2 shows the first four C_{ℓ}'s, which rapidly decrease in size with increasing ℓ. The dominant $C_0(x)$ is small at the origin because of the repulsion in V(x), while the remaining $C_{\ell}(x)$'s behave as $x^{2\ell}$ for small x. This means that only increasingly larger values of x contribute to the integrand in eqn. (5), which are suppressed by the finite range of the force. The values of $\langle V_{\ell} \rangle$ (for ℓ = 0, 2, ..., 10) for this simple potential model are given by [-36.6, -.163, -.019, -.002, -.0004, -.00008] MeV, dramatically illustrating the rapid convergence as ℓ increases. Clearly it should be sufficient to restrict ℓ to 4 or less. We will see later that this convergence rate also applies to more realistic potential models.

By expanding the potential in a series and then truncating the series after a reasonable number of terms, we have in effect reduced the problem to solving a set of coupled equations (for the partial waves) in two variables x and y, which makes the problem tractable. A good estimate of the time scale for numerically solving the deuteron problem, starting from scratch, is one or two months. The scale for the triton bound state is perhaps two years! The problem is still very difficult, and requires a substantial commitment of personal and computer time.

4. SCHRÖDINGER AND FADDEEV-NOYES EQUATIONS

We wish to solve a partial differential equation, the Schrödinger equation, for the triton bound state. It is sometimes forgotten by those who don't perform numerical calculations that such solutions require the imposition of well-defined boundary conditions. Simple bound-state problems only require the imposition of finiteness requirements for the wave function at the origin and at asymptotically large distances, where the wave function vanishes exponentially.

The scattering problem is more complex, and finiteness alone is not enough. Years ago, Foldy and Tobocman[8]) showed that the three-body Lippmann-Schwinger (LS) equation for scattering has no unique solutions, even when outgoing scattered waves are specified in the usual way. Even the two-body Lippmann-Schwinger equation has no unique solution, without further subsidiary conditions, if the problem is posed in a particular way! The problem we pose is: what is the outgoing-wave solution for two nucleons with a total energy of 20 MeV? This is a "trick" question, because we have deliberately not specified the center-of-mass (CM) motion of the two nucleons. As stated, an arbitrary linear combination of wave functions for a deuteron with 22.2 MeV CM energy, two nucleons in a $^1S_0$ threshold state with 20 MeV CM energy, and two nucleons with an internal energy of 10 MeV and 10 MeV CM energy solves the problem. Trivially, we can avoid the problem by working in the CM frame, which fixes the relative two-nucleon energy. Unfortunately, even in the CM frame of the three-nucleon problem this does not suffice, since the recoil of a third nucleon can compensate for the CM motion of the remaining pair in any state of internal motion commensurate with conservation of energy. Because of this, complicated phenomena are possible, which makes the ad hoc imposition of boundary conditions a dubious exercise. An incoming plane wave for a proton-deuteron system (pd) can scatter directly to a pd final state, or break up into a ppn final state, or the initial proton can pick up the neutron in the deuteron and that deuteron can escape. These many physical channels are not orthogonal and specifying outgoing waves is not enough.

Of particular importance is rearrangement, such as the neutron pickup example described above. We write the Schrödinger equation in the form

$$[E-(T+V_{12}+V_{13}+V_{23})]\Psi = 0 \quad , \tag{7}$$

where T, E, and V_{ij} are the kinetic energy, total energy, and potential energy for the pair (ij), respectively. If both V_{23} and V_{13} can support a deuteron bound state, an initial plane-wave state of nucleon 1 and bound nucleons 2 and 3 [denoted (1;23)] can asymptotically become nucleon 2 plus a bound (13) pair [(2;13)]; the converse is also true and both wave functions contain both physical processes. The difficulty is that while the LS equation specifies that the (1;23) configuration has an incoming plane wave and outgoing spherical wave, it does not rule out incoming plane waves for (2;13). In order to achieve a unique solution the LS equation must be supplemented by additional homogeneous equations, which is a cumbersome procedure.[9,10])

Faddeev[11]) provided the means to circumvent this dilemma. Although Faddeev's procedure was developed in momentum space, Noyes[12]) later cast that work into a physically equivalent configuration space form. We arbitrarily write

$$\Psi(\vec{x},\vec{y}) = \psi(\vec{x}_1,\vec{y}_1)+\psi(\vec{x}_2,\vec{y}_2)+\psi(\vec{x}_3,\vec{y}_3) \equiv \psi_1+\psi_2+\psi_3 \quad , \tag{8}$$

where the variables $(\vec{x}_i,\vec{y}_i)$ are the Jacobi coordinates defined earlier, and the function ψ in eqn. 8 is the same for all three terms. The original Schrödinger equation becomes three separate equations:

$$(E-T-V_{23})\psi_1 = V_{23}(\psi_2+\psi_3) \quad , \tag{9a}$$

$$(E-T-V_{13})\psi_2 = V_{13}(\psi_1+\psi_3) \quad , \tag{9b}$$

$$(E-T-V_{12})\psi_3 = V_{12}(\psi_1+\psi_2) \quad . \tag{9c}$$

Clearly, eqns. (9b) and (9c) are simply permutations of (9a), and we need solve only (9a). Since that equation involves only V_{23}(and not V_{13}) the problem of the rearrangement reaction has disappeared for ψ_1. It is contained in ψ_2. By this clever mechanism, Faddeev showed that

we only need to specify explicitly the much simpler boundary conditions for ψ_1, rather than for Ψ.

This is seen most clearly in fig. 3, where the regions of interest for the variables x and y are illustrated. The configuration (1;23) corresponds to an asymptotic state with $y \to \infty$, and $x < x_d$, the physical extent of the bound pair (23), and is denoted the "deuteron strip".

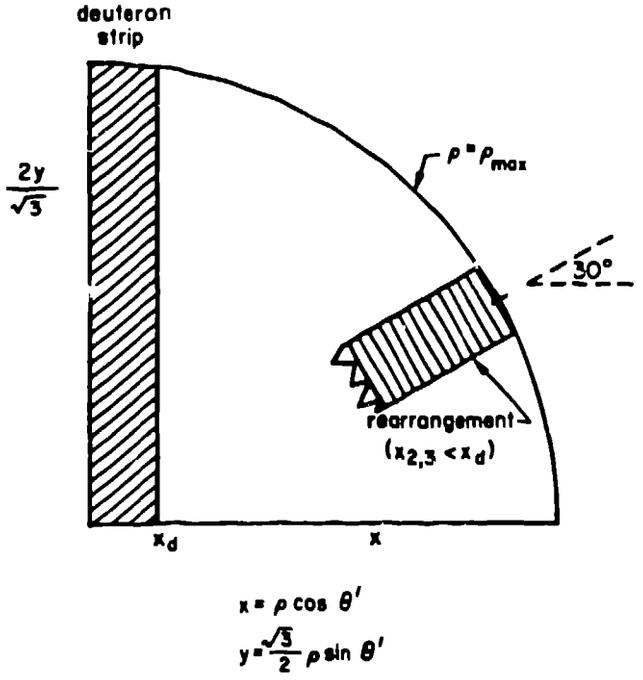

Figure 3. Configuration space regions for Nd scattering problem.

Rearrangement corresponds to small $x_2 = |\vec{r}_1 - \vec{r}_3|$ (i.e., a bound state in (13)) and this occurs when $\theta = 0$, and $\frac{2y}{\sqrt{3}} = x/2$ or $\theta' = 30°$ in terms of the polar coordinates

$$x = \rho\cos\theta' \quad , \tag{10a}$$

$$y = \frac{\sqrt{3}}{2}\rho\sin\theta' \quad . \tag{10b}$$

In complete analogy with the two-body problem, we can impose boundary conditions most easily for the reduced wavefunction

$$\phi_1 = xy\psi_1 . \tag{11}$$

In practice the region of the (x,y)-plane to the right of the deuteron strip is smooth for ϕ_1 and asymptotically behaves as

$$\phi_1^b \sim \frac{e^{iK\rho}}{\rho^{1/2}} f(\theta') \quad , \tag{12}$$

where f is an unknown angular function, while on the deuteron strip it behaves as

$$\phi_1^d \sim e^{iky} \phi_d(\vec{x}) \quad , \tag{13}$$

where $\phi_d(\vec{x})$ is the reduced deuteron wave function with energy $E_d = -\kappa_d^2/M$, k is the incident nucleon wave number, and K is $[3k^2/4-\kappa_d^2]^{\frac{1}{2}}$. Similar boundary conditions apply to the triton bound state case with $k \to i\kappa_d$ and $K \to i\kappa$. One enforces $\phi_1=0$ along x=0 and y=0, and $\phi_1 \sim \phi_1^b + \phi_1^d$ along the arc[13]) $\rho=\rho_{max}$.

These physical considerations can be seen graphically in fig. 4 and fig. 5 for $\theta=0$, which depict wave functions for the scattering of zero energy (k=0) neutrons and deuterons in the quartet spin state. The smooth function ψ_1 in fig. 4 has structure only along the deuteron strip, while fig. 5 depicts v_3, a component of the total wave function Ψ, which has structure along the deuteron strip and a ridge with "wings" along $\theta'=30^o$, which is the outgoing wave in the rearrangement channel.

The bound-state problem clearly has simpler boundary conditions[14]): we need only make the wave function vanish for some large $\rho=\rho_{max}$. Nevertheless, the Faddeev motivations for the scattering problem work equally well for the bound state, and we anticipate the Faddeev wavefunction ψ_1 will be smoother and easier to model numerically than Ψ. Indeed, the Illinois-Argonne group[2]) has recently found that incorporating the difference between the bound state analogues of eqns. (12) and (13) in their variational calculations

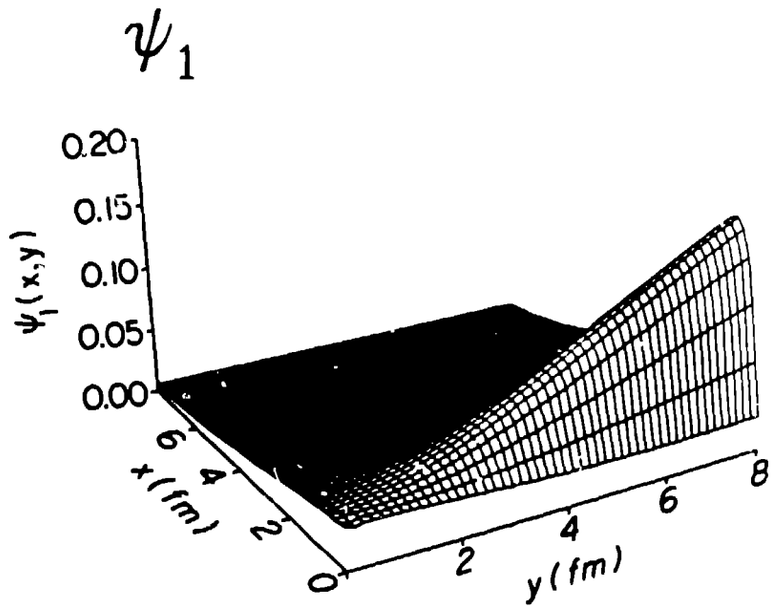

Figure 4. Faddeev wavefunction for quartet nd scattering, ψ_1, plotted versus x and y.

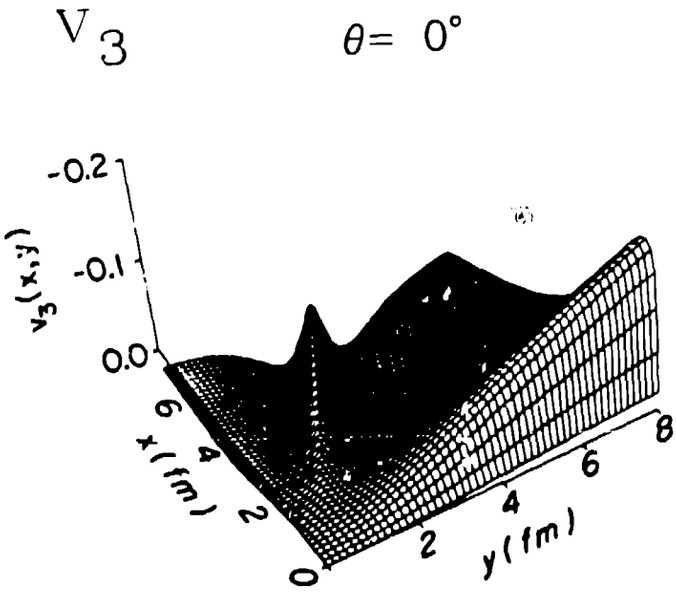

Figure 5. Schrödinger wavefunction component, v_3, for $\theta=0°$ generated from ψ_1 in fig. 4, plotted versus x and y.

(spin-triplet versus spin-singlet behavior along the deuteron strip) is quantitatively important.

5 NUMERICAL MODELLING

Having made the decision to partial-wave project the nucleon-nucleon force, it is necessary to determine the consequence of this for the Faddeev-Noyes equation. For simplicity we assume a force which is independent of spin and isospin and acts only in the s-wave. In terms of our previous discussion, such a force looks like $|0\rangle V(x)\langle 0|$, where the projector $|0\rangle$ refers to s-waves. This produces

$$\left[\frac{\partial^2}{\partial x^2} + \frac{3\partial^2}{4\partial y^2} - U(x) + K^2\right]\phi(x,y) = U(x)\int_1^1 d\mu \left[\frac{xy}{x_2y_2}\right]\phi(x_2,y_2), \quad (14)$$

where $U(x) = MV(x)/\hbar^2$, $\mu=\cos\theta$, and $\phi(x,y) = \frac{1}{2}\int_1^1 d\mu\phi_1(x,y,\mu)$. Note that ϕ does not depend on μ; it is completely independent of θ. Moreover, for the s-wave force chosen, all higher partial waves of ϕ_1 must vanish, because V vanishes for those waves, and therefore $\Psi(x,y,\mu) = \phi(x,y) + \phi(x_2,y_2) + \phi(x_3,y_3)$. This is an extremely important result, since all of the angular (μ) dependence in Ψ comes from the permuted terms, $\phi(x_2,y_2)$ and $\phi(x_3,y_3)$, and the computation of a 3-variable function has been reduced to one of only two variables. When many partial waves are computed, one has coupled equations in the two variables x and y. Nevertheless, the angular momentum barrier makes the required number tractable, and the calculation possible.

We still must make a choice of numerical methods in order to solve the equations. A technique which has proven exceptionally powerful in modern engineering applications is the finite element method, and its variant, the method of splines [5]. Figure 6 depicts at the top a function which we wish to approximate for computational purposes, between the points x_0 and x_4, and for demonstration purposes we choose to do so by dividing the distance into 4 equally spaced regions or intervals. The finite element method consists of approximating the function in each interval by a (different) polynomial of order N and forcing the function and its first m derivatives to be continuous at

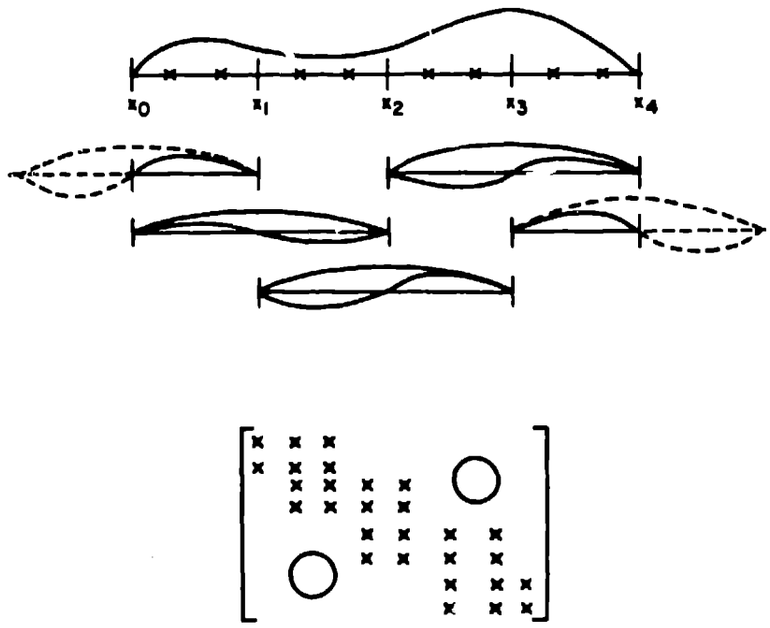

Figure 6. The function at the top is approximated by the sum of 5 spline functions in the middle. The use of such splines with a second-order differential equation leads to the banded matrix shown at the bottom.

the "break points" between intervals. For definiteness we will choose cubic splines (N=3) involving 4 parameters, and force the function and its first derivative to be continuous. There are a total of 16 parameters, and two imposed conditions at each of 3 breakpoints, leaving 10 free parameters. The function is chosen to vanish at the endpoints, leaving 8 parameters which are chosen so that at two "collocation" points (indicated by x's) in each of the 4 intervals the function agrees exactly with the function we are modelling. If we are solving an equation for this function, we force the equation to be exactly satisfied at those points.

An alternative scheme is to use splines, which eliminates much of the labor. The finite elements in a given interval are grouped with those in a neighboring interval, which are then overlapped as shown in the middle of the figure. That is, at any point, x, the function is

approximated as the sum of two overlapping functions, each defined in a double interval. These spline functions and their first m derivatives are required to vanish at the right and left ends of the double interval and to be continuous at the middle boundary. For our case (N=3 and m=1) the 8 finite element parameters for any double interval are reduced to two by these six conditions. We have graphed these (Hermite) splines as even and odd functions in the double interval, and the remaining parameters are simply the overall strengths of each of these functions. The beauty of this scheme is that the use of overlapping splines now guarantees that the function and its first derivative are continuous without any extra work! The boundary conditions are trivially satisfied by making the even function in the end intervals vanish, and the remaining 8 parameters in the 5 overlapping spline functions are determined at the collocation points, as before. The strength of this method is that the overall number of unknowns has been reduced to the minimum before we even set up matrix equations.

The orthogonal collocation method allows one to choose the collocation points so that the power of Gauss quadratures and splines can be combined[16]). If we were to perform an integral over the function in the figure, a natural way to do this would be to integrate between break points and use a Gauss quadrature formula in each interval. Using those quadrature points as collocation points constitutes the method of orthogonal collocation, which substantially improves rates of convergence when solving equations using splines.

Because splines are local functions, separately defined in each double interval, the collocation conditions couple splines from neighboring intervals only. The complete set of such conditions for all parameters (8 in our example) constitutes a matrix equation, and this matrix has a very special form because of the locality; it is a band matrix, with most of the elements zero, as shown at the bottom of fig. 6. Such matrices are much easier to invert than dense matrices, and should be preserved, if possible. In order to deal with the angular integral in eqn. 14, we transform from (x,y) coordinates to the polar coordinates (ρ,θ'). The integral destroys the double "band" structure in x and y; polar coordinates preserve this structure in the variable ρ.

There are a number of important advantages which accrue from using splines to model a function: (1) The spline approximant and a specified number of derivatives are automatically continuous; (2) The splines automatically provide an interpolating function at any point; (3) They lead to a band matrix; (4) They are "optimally" smooth; (5) It is easy to change from the equally spaced intervals of our example to any desired distribution; (6) The splines are easy to program on a computer; (7) Boundary conditions are easy to impose; (8) The approximants exactly satisfy the constraint equations at the collocation points; (9) Piecewise local functions such as splines do not propagate approximation errors, as global functions do; (10) The relative accuracy of the wave function and the eigenvalue should be comparable. We also note that the use of overlapping double intervals corresponds closely to one derivation of the powerful Gregory's integration rule from Simpson's integration rule.

6. TWO-BODY AND THREE-BODY FORCES

6.1 Two-Body Force Results

There is little difference in principle between solving eqn. (14) for a single nucleon-nucleon (NN) partial wave and using many partial waves. The size of the matrices becomes much larger, and the matrix bookkeeping becomes very tedious and intricate. In general for each nucleon-nucleon partial wave, there are two spectator partial waves associated with the two spin states of the latter, except for total angular momentum, J, equal to zero, which generates only one. The four NN partial waves ($^{S}L_{J}$) for each J ($^{1}J_{J}$, $^{3}J_{J}$, $^{3}J\text{-}1_{J}$, $^{3}J\text{+}1_{J}$) thus generate 8 trinucleon channels, except for J=0, which has only two, associated with $^{1}S_{0}$ and $^{3}P_{0}$. As we indicated earlier, the $^{1}S_{0}$ and $^{3}S_{1}$ waves should be dominant, and we must also include the $^{3}D_{1}$ wave, which is strongly coupled by the tensor force to the $^{3}S_{1}$ wave. This combination is the standard 5-channel calculation (all positive-parity NN waves with $J\leq 1$), while 9 and 26 channels constitute all positive-parity NN waves with $J\leq 2$ and $J\leq 4$, respectively. The 18- and 34-channel cases use all NN partial waves with $J\leq 2$ and $J\leq 4$.

A brief summary of results[14]) for the Reid Soft Core (RSC)[18]), Argonne V_{14} (AV14)[19]), Super-Soft-Core(C) [SSC(C)][20]), and Paris[21]) potential models is given in Table 1 as a function of channel number. Several conclusions are obvious: (1) The 5-channel approximation gives most of the binding (within .2-.3 MeV); (2) The negative-parity NN waves don't have a large effect; (3) The binding is roughly 1 MeV below experiment; (4) The point-nucleon rms charge radii (i.e., the proton radii) for ^{3}He and ^{3}H are larger than experiment. Because the positive-parity waves dominate, this table doesn't demonstrate the rate of convergence of the partial-wave series. This is shown in Table 2 for the RSC 34-channel case, where <V> is broken down into contributions for fixed J and fixed parity. All but 1% of the total potential energy (indicated by Σ in the last column) is generated by the first 5 channels, and most of the rest from the remaining positive-parity waves. The small negative-parity NN forces give 200 keV more binding, which is not obviously reflected in Table 1 (compare 18 channels to 9 channels). The reason is that the negative-parity forces couple directly to the small components of the wave function and this leads to nearly cancelling contribution from first- and second-order perturbation theory. First-order perturbation theory works well for all the other small components.

The probabilities of the important S'- and D-state wave function components are small. The D-state probabilities for the triton are very nearly 3/2 times the corresponding D-state probability of the deuteron for each potential model.

Table 1. Binding energies, point charge radii in fm, and wave function component percentages for various two-body force models[17]).

	-E (MeV)					$\langle r^2\rangle^{\frac{1}{2}}_{He}$	$\langle r^2\rangle^{\frac{1}{2}}_{H}$	$P_{S'}$	P_D
Model	5	9	18	26	34	34	34	34	34
RSC	7.02	7.21	7.23	7.34	7.35	1.85	1.67	1.40	9.50
AV14	7.44	7.57	7.57	7.67	7.67	1.83	1.67	1.12	8.96
SSC(C)	7.46	7.52	7.49	7.54	7.53	1.85	1.68	1.24	7.98
Paris[22])	7.30		7.38						
Expt.		8.48				1.69(3)	1.54(4)	--	--

Table 2. Potential energies (in MeV) for the RSC 3a-channel case broken down according to J (total nucleon-nucleon angular momentum) and parity, and the kinetic energy for comparison.

J	0	1	2	3	4	Σ
$\langle V_J \rangle$	-13.729	-43.647	-0.435	-0.115	-0.020	-57.946
$\langle V_J^+ \rangle$	-13.553	-43.874	-0.188	-0.117	-0.014	-57.746
$\langle V_J^- \rangle$	-0.176	0.227	-0.247	0.002	-0.006	-0.200
$\langle T \rangle$						50.600
$\langle H \rangle$						-7.345

6.2 Three-Body Forces

6.2.1 Motivation and Evidence

Our results strongly indicate that there is a defect in binding from conventional two-body forces. Moreover, the too large (calculated) radii are likely a symptom of this same problem. There are several plausible explanations: (1) Relativistic corrections have not been calculated; (2) Three-body forces, which depend on the simultaneous coordinates of all 3 nucleons in the triton, have not been included; (3) Our model Hamiltonians are simply inadequate, and the effects of nucleon structure or meson degrees of freedom should be taken into account. In fact, these categories are not distinct. Relativistic corrections can be broken down into one-body (kinetic energy) terms, two-body (potential) terms, and three-body (and higher) potential terms. The size estimate we previously made of relativistic corrections, (1-few percent) taken for the kinetic or potential energies (±50 MeV) predicts a scale of 0.5-1 MeV. Those calculations that have been performed on the one- and two-body parts are consistent with this estimate, but find a tendency for cancellation between the attractive kinetic energy correction and a repulsive potential energy correction, leaving a small residue. It is also known[4,23]) that a substantial part of the two-pion-exchange three-body force is a

relativistic correction of order V_π^2/Mc^2, where V_π is the usual one-pion-exchange potential (OPEP). Moreover, the conceptually important isobar part[24]) of the former force is due to nucleon substructure: a pion emitted by nucleon 1, (virtually) polarizes nucleon 2 into an isobar, which decays back to a nucleon plus a pion, which is absorbed by nucleon 3. Most of the currently popular three-nucleon forces have been derived by considering meson degrees of freedom. These forces clearly exist in nature, but are they large enough to solve our problem? Before discussing the results of various calculations, we consider possible additional evidence.

One long-standing problem has been a good theoretical understanding of the ^{3}He charge form factor, or the Fourier transform of the charge density. The form factor has a typical diffraction shape, as a function of q, the momentum transfer, falling rapidly through zero, becoming negative in the secondary maximum, and then positive again. The difficulty has been that theoretical calculations have predicted too small a (negative) strength in the secondary maximum. The point-nucleon charge density $\rho_{ch}(r)$ constructed from the experimental form factor $F_{ch}(q^2)$ is consequently much lower than theoretical calculations near the origin[4]), as shown in fig. 7. This follows from

$$\rho_{ch}(0) = \frac{1}{2\pi^2} \int_0^\infty F_{ch}(q^2) q^2 dq \quad . \tag{15}$$

Clearly, a large negative contribution to F_{ch} lowers $\rho_{ch}(0)$. The argument that we have presented is somewhat controversial, because values of F_{ch} for very large q are needed in order to make the integral converge, and this requires considerable theoretical assumptions and extrapolation, some of which may be dubious. Nevertheless, there is a problem with the form factor.

In impulse approximation, the charge density measures the probability of finding a proton at a distance r from the trinucleon center-of-mass, indicated by the x in fig. 1. Taking nucleon 1 to be that proton, we have $r = \frac{2}{3}y$, and forcing r to zero makes y zero. This is the condition for all three nucleons existing in a collinear configuration. Binding, on the other hand, prefers equilateral or isos-

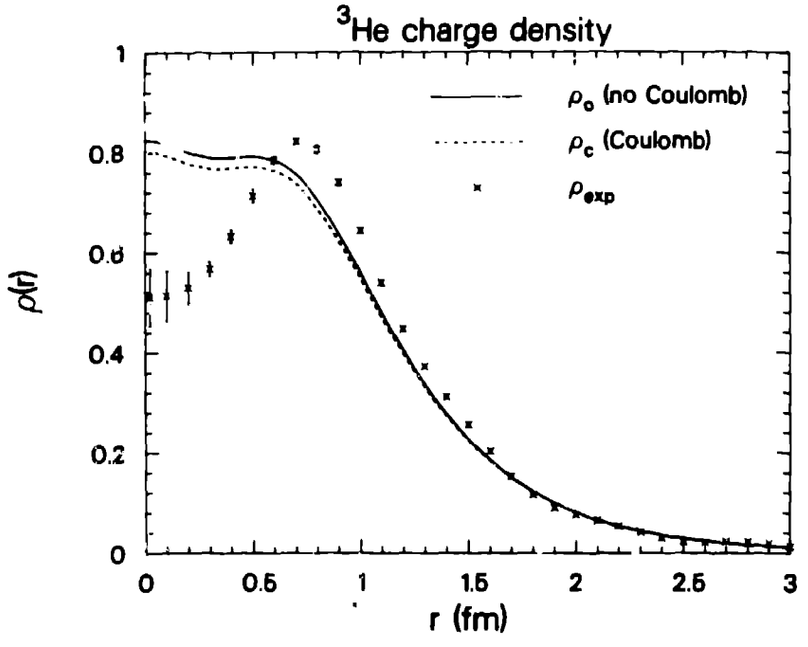

Figure 7. Experimental (x's) and theoretical charge densities for ^{3}He. The theoretical curves correspond to including or not including a Coulomb force between the protons in ^{3}He.

celes configurations, so that each nucleon can be attracted by the short-range force of each of the other nucleons. Both of our problems with experiment could be solved if the three-nucleon force were attractive for equilateral configurations and repulsive for collinear ones. Schematic models of the force have this structure, and produce both effects, altnough other models do not.

In addition to bound states, the trinucleons have a rich continuum structure. At very low (essentially zero) energy the scattering of a nucleon from the deuteron can be characterized by a single observable, the scattering length, a, which can be decomposed into spin-doublet (a_2) and spin-quartet (a_4) components. The latter is quite uninteresting, because it seems to depend only on the deuteron's binding energy; consequently, all "realistic" force models produce nearly the same result. Calculations of the doublet scattering length, on the other hand, have been too large. Typical values[25]) are shown in fig. 8, where a_2 has been calculated for a variety of realistic and

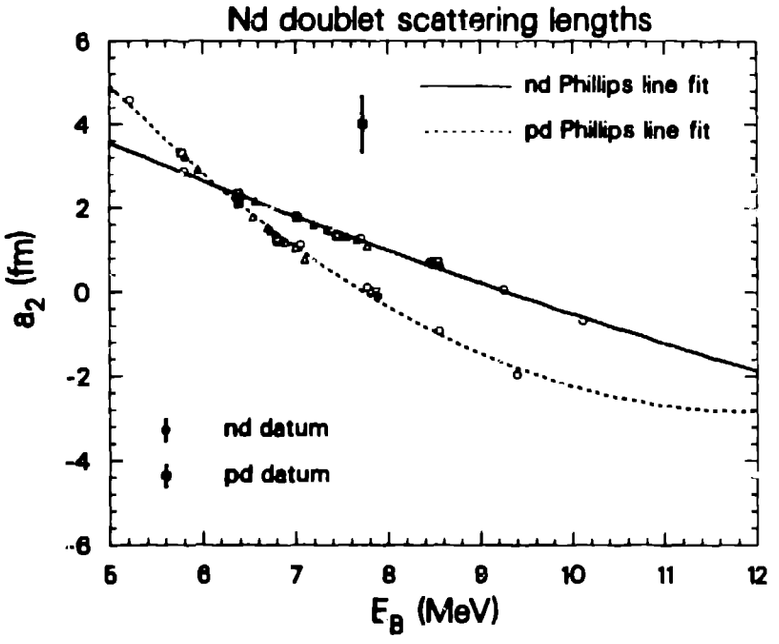

Figure 8. Doublet nd and pd scattering length plotted versus ^{3}He and ^{3}He binding energies, respectively. Individual points are from theoretical calculations (triangles, squares, and circles correspond to realistic two-body force models, the additional inclusion of three-body forces, and unrealistic two-body force models).

unrealistic two- and three-body force models. These np and pd scattering results separately fall on "Phillips lines" when plotted versus the corresponding triton or ^{3}He binding energy[26]). The fit to the nd results passes through the experimental datum; the pd result does not, which is a mystery at this time. The fact that all of the nd doublet results track the same Phillips line indicates that whatever physical mechanism corrects the binding defect will also produce a correct value for a_2, at least for the nd case.

Finally, analyses of the nn-scattering length, a_{nn}, from two separate experiments, n+d→(n+n)+p and π^-+d→(n+n)+γ, have produced three different values of a_{nn}. It has been argued[27]) that three-nucleon forces, conspicuously missing in the latter reaction and not included

in the analyses of the former reaction, might produce agreement among the values of a_{nn} from the different reactions. Only schematic calculations have been performed to date[28]).

6.2.2 Bound state calculations.

The evidence we have presented is tantalizing, but circumstantial. At present the best evidence exists in the properties of the bound state. Can current models of the three-nucleon force produce a substantial increase in binding? At least four such models have been used recently: (1) the Tucson-Melbourne (TM) two-pion-exchange force[29]); (2) the Brazilian (BR) two-pion-exchange force[30]); (3) the Urbana-Argonne (UA) schematic force[31]); (4) the Hajduk-Sauer isobar model[32]). Hajduk and Sauer do not explicitly include a separate three-body force in their model, but rather include isobar components in their wavefunctions. Three-body force contributions, implicitly included in their model, must be deduced later.

The early calculations used different force models and various approximations which resulted in a chaotic situation, some calculations finding negligible additional binding and others finding more than one MeV. The situation has recently been clarified in part[33]). Most calculations have resorted to perturbation theory using 5-channel wave functions[34]), which fails badly. Perturbation theory is inadequate for the TM model, giving results which are much too small. The 5-channel wave function approximation is also inadequate in general, as noted by Hajduk and Sauer[22,32]), because the pion-exchange vertices induce large couplings to small wave function components not adequately represented in the 5-channel approximation; 34 channels are required for complete convergence[35]). The latter calculations found approximately 1.5 MeV additional binding from both the TM and BR forces, in combination with two different two-body force models. Calculations of $\rho_{ch}(0)$ were not completed.

Although these results indicate a substantial effect, caution is required. Hajduk and Sauer find a small (-.3 MeV) three-body force effect. Their approach is very different from the TM and BR groups, and the physical reasons for the discrepancy are not known. Moreover, the "long-range" two-pion-exchange force is unfortunately quite sen-

sitive to its short-range behavior, and it is possible to substantially lower the binding by making plausible modifications of this behavior. This field is in its infancy and much more work needs to be performed.

7. SUMMARY AND CONCLUSIONS

7.1. Scaling of Observables

Although a wide variety of bound state calculations have been performed during the previous two decades for a variety of potential models, many produced only binding energies and no wave functions, and others required approximations whose reliability was difficult to assess. The recent studies of the Los Alamos-Iowa group[35]) have produced a large number of numerically accurate triton wavefunctions for four different two-body potential models in combination with several different three-body force models, each calculated for various numbers of channels. Although there is no guarantee that these model combinations accurately describe nature, the solutions at least incorporate the correct quantum mechanical constraints. Moreover, the binding energies for the set of models extend from below to above the physical binding energy of the triton. This provides us for the first time with the opportunity to investigate how a variety of important ground state observables depend on the binding energy, and whether there is any model dependence as well. We saw a very important illustration of this in the Phillips line, which appears to systematize the behavior of the doublet scattering length results.

What are the important ground state properties, besides the binding energy? A list of the most commonly calculated ones would include the (point) charge radii, $\langle r^2 \rangle^{\frac{1}{2}}_{He}$ and $\langle r^2 \rangle^{\frac{1}{2}}_{H}$, the probabilities of the various wave function components (which are not measurable), the Coulomb energy of ^{3}He, E_c, the magnetic moments of ^{3}He and ^{3}H, the asymptotic norms (sizes of asymptotic wave function components), and the β-decay matrix element of ^{3}H. The magnetic moments depend on meson-exchange currents and on the S'- and D-state probabilities, P_S' and P_D, as does the β-decay matrix element; we will not discuss them further. The asymptotic norms depend on binding, but this has not been assessed in detail yet. The radii and Coulomb energy depend sensitively

on the binding energy, and calculations of these observables which use models that underbind will produce inadequate predictions. We assess the status of these important physical quantities below, together with simple qualitative arguments that account for our conclusions.

For pedagogical purposes, the difference of the ^{3}He and ^{3}H charge radii can be understood in terms of the oversimplified pictures in fig. 9. The sketch at the top depicts a schematic ^{3}He when the nucleon-

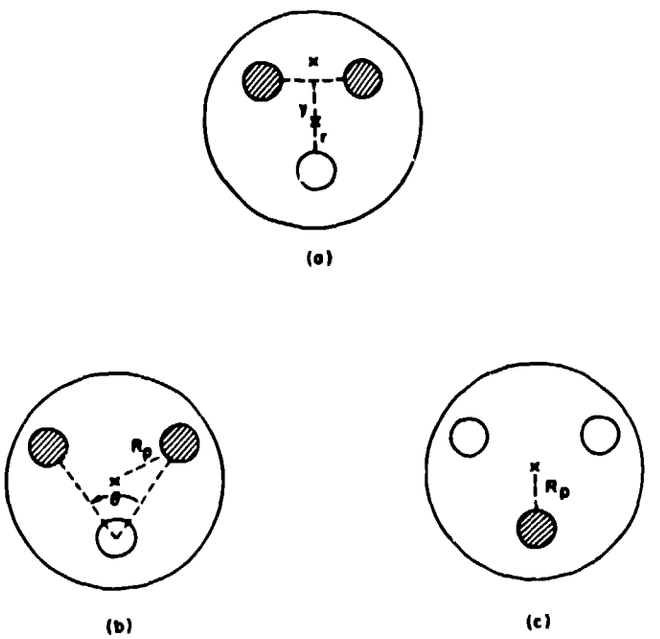

Figure 9. Schematic trinucleons with identical forces between protons (shaded) and neutrons in (a) and with different forces for ^{3}He in (b) and ^{3}H in (c).

nucleon forces between all pairs are identical. This is represented by an equilateral triangle configuration, with shading depicting the protons. The charge or proton radius, R_p, measures the integrated probability of finding a proton at a distance r from the center-of-mass. In this simple example, the proton, neutron, and mass radii are

all the same. When the forces between pairs are different, the appropriate pictures for ^{3}He and ^{3}H are those of fig. (9b) and fig. (9c). The np forces are stronger than the nn or pp ones (only the np system has a two-body bound state) and this allows the protons in ^{3}He and the neutrons in ^{3}H to lie further from the center-of-mass than their counterparts (i.e., $\theta>60°$). The resulting isosceles configuration is reflected in the appearance of an S'-state, which directly measures the isosceles-equilateral difference, and in the fact that R_p for ^{3}He increases, while that of ^{3}H decreases, and hence $\langle r^2\rangle^{\frac{1}{2}}_{He} > \langle r^2\rangle^{\frac{1}{2}}_{H}$, irrespective of any pp Coulomb force in ^{3}He.

These arguments can be made quantitative by decomposing the mean-square-radius in impulse approximation into isospin components[36]): the isoscalar part $\langle r^2\rangle_s$ mirrors fig. (9a) and is determined by sums of squares of wave function components. The isovector component contains one part proportional to the isoscalar component and another part largely determined by the overlap of the S- and S'-states, which we denote $\langle r^2\rangle_v$ (v does <u>not</u> mean isovector), and determines the difference between ^{3}He and ^{3}H. One finds for ^{3}He (Z=2) and ^{3}H(Z=1), with upper and lower signs, respectively,

$$Z\langle r^2\rangle = Z\langle r^2\rangle_s \pm \langle r^2\rangle_v \quad . \tag{16}$$

These quantities have very different behaviors. Radii in general are sensitive to the asymptotic parts of the wavefunction. If one assumes that the entire wavefunction is represented by the bound-state analogue of eqn. (12), one finds that

$$\langle r^2\rangle^{\frac{1}{2}}_s = \frac{1}{2\kappa} \sim E_B^{-\frac{1}{2}} \quad . \tag{17}$$

Figure 10 shows the results of calculating $\langle r^2\rangle^{\frac{1}{2}}_s$, and $\langle r^2\rangle^{\frac{1}{2}}_v$, together with the experimental data[4]) corrected for the nucleons' finite size. The fit to the scalar points is accurately represented by $.8E_B^{-.5}$, indicating that our simple argument was essentially correct. The difference radius is fit by $.14E_p^{-.9}$, and this different behavior reflects different physics. Clearly , the amount of S'-state plays a significant role. The percentage of S'-state is plotted versus binding

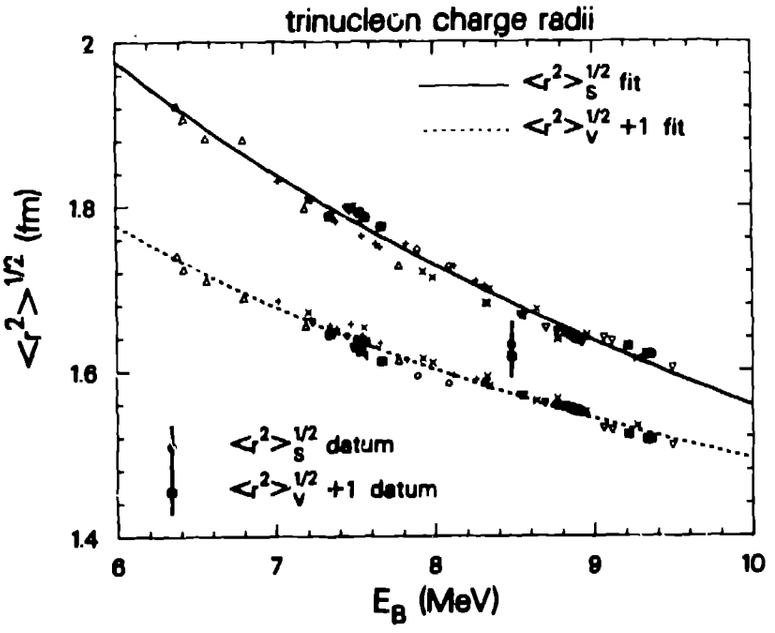

Figure 10. Calculated trinucleon (point nucleon) rms charge radii decomposed into isoscalar (s) and difference (v) contributions in impulse approximation, together with data, plotted versus corresponding binding energy. The ^{3}He calculations contained no Coulomb force.

energy in fig. 11, and the fit varies as $E_B^{-2.1}$ This decrease is expected, because as binding increases only the average force is important, and the np-nn difference is less important. In a simple harmonic oscillator description, the S'-state is given in terms of excited state configurations, which decrease $\sim E_B^{-2}$ as the oscillator spacing increases with binding. Finally, the ^{3}He and ^{3}H results are shown in fig. 12. If the small discrepancies between theory and experiment are real, they probably reflect a small breakdown of the impulse approximation.

The Coulomb force $V_c(x)$ between protons in ^{3}He is quite weak and can be accurately treated in perturbation theory. The second-order Coulomb effect[37]) is estimated to be ~-4 keV, compared to a ^{3}He-^{3}H binding energy difference of 764 keV. Since $V_c \sim 1/R$, schematically, and since $R \sim E_B^{-\frac{1}{2}}$, we expect E_c to scale roughly as $E_B^{\frac{1}{2}}$. A better

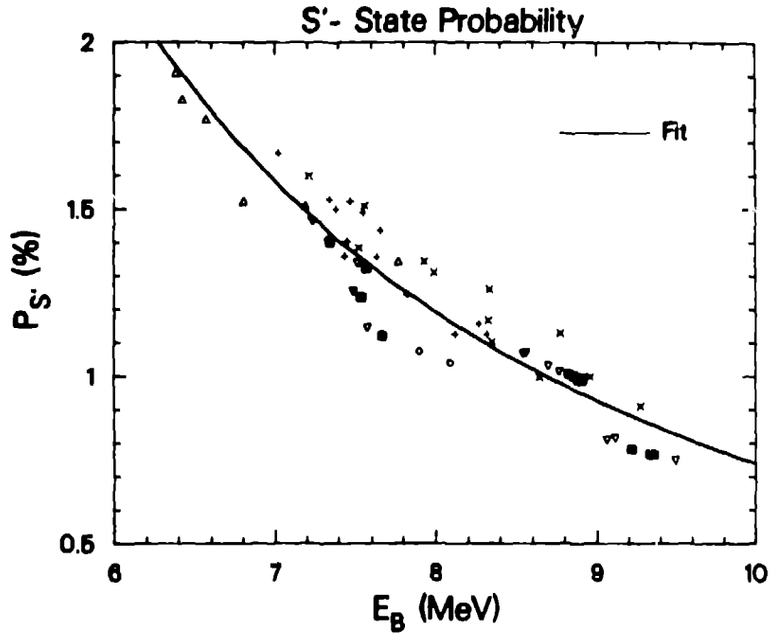

Figure 11. Calculated trinucleon S´-state percentages plotted versus corresponding binding energy.

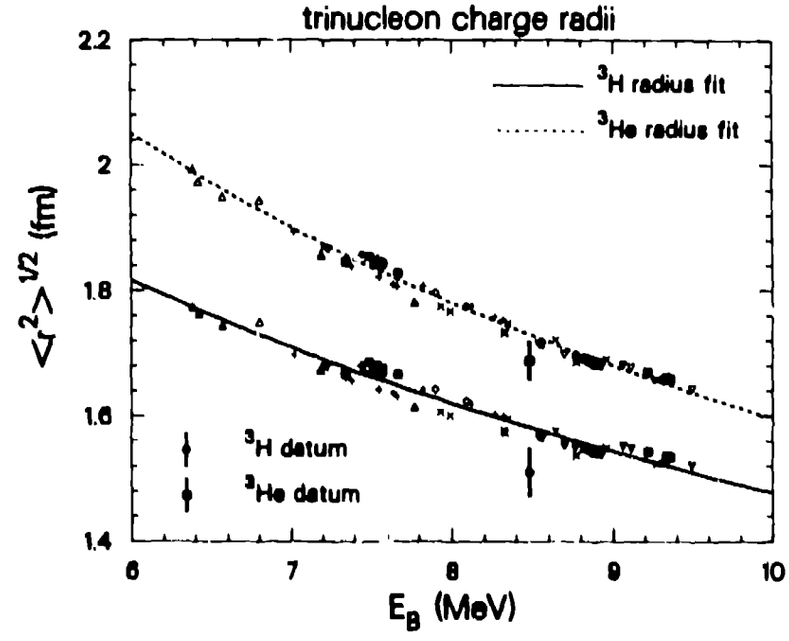

Figure 12. Calculated trinucleon (point nucleon) rms charge radii in impulse approximation, plotted versus corresponding binding energy. The ^{3}He calculations contained no Coulomb force.

description is available, however, if we utilize fig. (9a). In this schematic ^{3}He the distance x between protons is given by $\sqrt{3}r$, and thus $E_c = \langle V_c(x)\rangle = \alpha\langle 1/r\rangle/\sqrt{3}$, where α is the fine structure constant. Consequently[38,39],

$$E_c \cong \frac{\alpha}{\sqrt{3}}\int\frac{d^3r}{r}[\rho_s(r) + \rho_v(r)]g(r) \equiv E_c^H \quad , \tag{18}$$

where we have added the effect of nucleon finite size, g(r), and written the matrix element in terms of the scalar and difference charge densities. The accuracy of this hyperspherical approximation is demonstrated in fig. 13. Although a priori a very implausible approximation, E_c^H overestimates E_c by only 1 percent. This is an important result, because the charge densities are experimentally measurable. Using these data[36] one finds E_c = 638 ± 10 keV. This is significantly less than the binding energy difference and reflects the existence of nonnegligible charge-symmetry-breaking forces other than the Coulomb interaction.

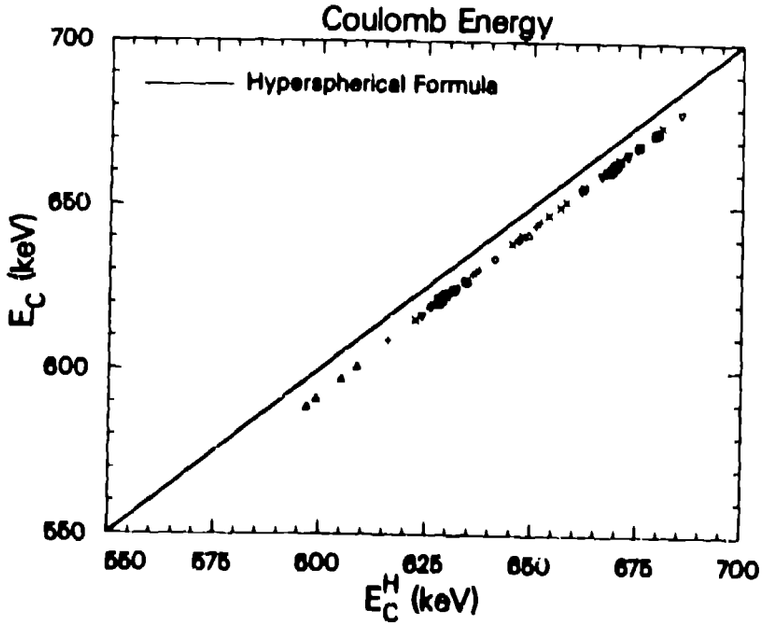

Figure 13. ^{3}He Coulomb energy, E_c, plotted versus the corresponding hyperspherical approximation, E_c^H.

7.2 Conclusions

Rapid and significant advances have been made in the few-nucleon problem recently. Many aspects of the bound states, including the Coulomb energy and charge radii, are now fairly well understood. The Phillips line connection between the doublet scattering length and the triton binding energy has been demonstrated with three-body forces. Many long-standing problems may be capable of resolution in the near future.

Although we have concentrated on the trinucleon bound states, the continuum is also important. Photonuclear reactions necessarily break up the triton and ^{3}He, and this is an important area of study. The continuum problem above breakup threshold is much more complicated than the bound-state problem, because the boundary conditions are difficult to implement in a tractable way. Nevertheless, the future of three-body physics lies in this regime.

Figure 14 shows a possible scheme[40]) for determining the size of three-body forces by exploiting its angular dependence in the continuum. The initial pd configuration can be broken up into a p+p+n final state, which is measured in an equilateral configuration (b) and in a collinear one (c). This very difficult experiment might shed light on such forces, by looking for the expected additional attraction in the former configuration and repulsion in the latter.

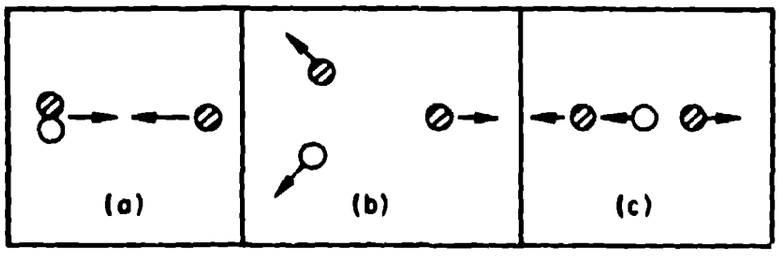

Figure 14. Scenario for probing three-nucleon forces with pd initial state (a) becoming equilateral (b) and collinear (c) three-body breakup configurations.

7.3 Acknowledgements

This work was performed under the auspices of the U. S. Department of Energy. The assistance of my collaborators, G. L. Payne, B. F. Gibson, and C. R. Chen, in preparing this lecture was deeply appreciated.

REFERENCES

1) Bethe, H. A. and Bacher, R. F., Rev. Mod. Phys. 8, 82 (1936).
2) Schiavilla, R., Pandharipande, V. R., and Wiringa, R. B., to be published.
3) Ballot, J. L. and Fabre de la Ripelle, M., Ann. Phys. (N. Y.) 127, 62 (1980).
4) Friar, J. L., Gibson, B. F., and Payne, G. L., Ann. Rev. Nucl. Part. Sci. 34, 403 (1984).
5) Kalos, M. H., Phys. Rev. 128, 1791 (1962).
6) Friar, J. L., Tomusiak, E. L., Gibson, B. F., and Payne, G. L., Phys. Rev. C 24, 677 (1981).
7) Malfliet, R. S. and Tjon, J. A., Nucl. Phys. A127, 161 (1969).
8) Foldy, L. L. and Tobocman, W., Phys. Rev. 105, 1099 (1957).
9) Glöckle, W., Nucl. Phys. A141, 620 (1970).
10) Payne, G. L., Klink, W. H., Polyzou, W. N., Friar, J. L., and Gibson, B. F., Phys. Rev. C 30, 1132 (1984).
11) Faddeev, L. D., Zh. Eksp. Teor. Fiz. 39, 1459 (1960).
12) Noyes, H. P., in "Three Body Problem in Nuclear and Particle Physics," edited by J. S. C. McKee and P. M. Rolph (North-Holland, Amsterdam, 1970), p. 2.
13) Glöckle, W., Nucl. Phys. A141, 620 (1970).
14) Payne, G. L., Friar, J. L., Gibson, B. F., and Afnan, I. R., Phys. Rev. C 22, 823 (1980).
15) Prenter, P. M., "Splines and Variational Methods" (Wiley, New York, 1975).
16) De Boor, C. and Swartz, B., SIAM (J. Num. Anal.) 10, 582 (1973).
17) Chen, C. R., Payne, G. L., Friar, J. L., and Gibson, B. F., Phys. Rev. C 31, 2266 (1985).

18) Reid, R. V. Jr., Ann. Phys. (N. Y.) 50, 411 (1968).

19) Wiringa, R. B., Smith, R. A., Ainsworth, T. A., Phys. Rev. C 29, 1207 (1984).

20) de Tourreil, R. and Sprung, D. W. L., Nucl. Phys. A201, 193 (1973).

21) LaCombe, M., Loiseau, B., Richard, J. M., Vinh Mau, R., Côte, J., et al., Phys. Rev. C 21, 861 (1980).

22) Hajduk, C. and Sauer, P. U., Nucl. Phys. A369, 321 (1981).

23) Friar, J. L. and Coon, S. A., Phys. Rev. C (to be published).

24) Hajduk, C., Sauer, P. U., Strueve, W., Nucl. Phys. A405, 581 (1983).

25) Friar, J. L., Gibson, B. F., Payne, G. L., and Chen, C. R., Phys. Rev. C 30, 1121 (1984); and to be published.

26) Phillips, A. C., Rep. Prog. Phys. 40, 905 (1977).

27) Slaus, I., Akaishi, Y., Tanaka, H., Phys. Rev. Lett. 48, 993 (1982).

28) Bömelburg, A., Glöckle, W., Meier, W., in "Few Body Problems in Physics," Vol. II, ed. by B. Zeitnitz (North-Holland, Amsterdam, 1984), p. 483.

29) Coon, S. A., Scadron, M. D., McNamee, P. C., Barrett B. R., Blatt, D. W. E., McKellar, B. H. J., Nucl. Phys. A317, 242 (1979).

30) Coelho, H. T., Das, T. K., Robilotta, M. R., Phys. Rev. C 28, 1812 (1983).

31) Carlson, J., Pandharipande, V. R., and Wiringa, R. B., Nucl. Phys. A401, 59 (1983).

32) Hajduk, C. and Sauer, P. U., Nucl. Phys. A322, 329 (1979).

33) Chen, C. R., Payne, G. L., Friar, J. L., and Gibson, B. F., Phys. Rev. Lett. (to appear).

34) Wiringa, R. B., Friar, J. L., Gibson, B. F., Payne, G. L., Chen, C. R., Phys. Lett. 143B, 273 (1984).

35) Friar, J. L., Gibson, B. F., Chen, C. R., and Payne, G. L., Phys. Lett. (to appear).

36) Friar, J. L. and Gibson, B. F., Phys. Rev. C 18, 908 (1978).

37) Payne, G. L., Friar, J. L., and Gibson, B. F., Phys. Rev. C 22, 832 (1980).

38) Friar, J. L., Nucl. Phys. A156, 43 (1970).

39) Fabre de la Ripelle, M., Fizica 4, 1 (1972).

40) Friar, J. L., AIP Conference Proceedings 97, 378 (1983).